

Common-Mode Frequency of Power Systems Affected by Voltage Dynamics

Huisheng Gao, Huanhai Xin, Guang Hu, Bin Cao, Hui Yuan, Linbin Huang

Abstract—The increasing penetration of converter-interfaced generators (CIGs) in power systems has posed great challenges in frequency stability analysis, as the frequency dynamics of CIGs may be strongly coupled with voltage dynamics. However, existing analytical models for system frequency generally cannot precisely account for the impact of voltage dynamics, leading to potentially incorrect results. The main challenge here is how to understand system frequency in the case of non-constant bus voltages, and how to integrate the voltage dynamics of devices at different bus locations into the system frequency model. To address this issue, this article defines the voltage-influenced common-mode frequency (VCMF), serving as a system frequency analysis model considering voltage dynamics. The VCMF is derived through the decomposition of bus frequency responses, leveraging the connection between the consistent part of bus frequencies and the rotational invariance of power flow. The decomposition process introduces voltage dynamics of devices into the system frequency response, represented as a global term that interconnects all devices through the power network. To address the complexity of this global term, an algebraic graph theory-based network partitioning method is introduced. This method effectively divides the globally coupled term into several locally coupled components, making the analysis of the VCMF more manageable. Finally, simulations are used to validate the proposed methods and confirm their validity.

Index Terms—Frequency stability, voltage-influenced common-mode frequency (VCMF), system frequency model, voltage dynamics, network partitioning.

I. INTRODUCTION

Power systems are experiencing rapid development due to the large-scale integration of renewable energy sources that are connected to power grids via power electronic converters. The low inertia and weak frequency regulation capability of Converter-Interfaced Generators (CIGs) pose great challenges to the frequency stability of power systems [1]. Notably, recent blackouts in England and Texas have demonstrated the vulnerability of system frequency, leading to substantial frequency deviations and necessitating widespread load shedding [2], [3]. Therefore, it becomes imperative to conduct a comprehensive analysis of the frequency responses of modern power systems to support the rapid development of renewable energy sources.

While bus frequency responses of power systems exhibit spatial variations, frequency stability analysis predominantly focuses on the consistent part of bus frequencies, namely the system frequency (also known as global frequency); see, for instance, the frequency stability analysis in the recent IEEE power system stability classification [4]. To analyze the system frequency, there are two primary categories of methods: simulation-based and analytical approaches [5]. Simulation-based method requires the construction of complex high-order models for the whole power system. While this approach

provides a high level of accuracy, it lacks mechanism explanations. Furthermore, conducting simulations under various conditions can be computationally demanding. Conversely, analytical approaches generally rely on relatively low-order models. They offer deeper physical insights, demand fewer computational resources, and have gained extensive utilization in practice [6].

Since the system frequency represents the consistent part of bus frequencies, it is intuitive to establish an equivalent single-generator system model to simplify the analysis. To achieve this, it is necessary to address two fundamental and well-connected questions: What exactly is the system frequency, and how can various devices at different buses be integrated into a single-generator model?

Regarding the first question, the Center of Inertia (CoI) is a widely-acknowledged method for defining and understanding system frequency. By combining swing equations of all generators in a power system, we can determine the CoI frequency with an equivalent single generator, whose inertia, mechanical, and electrical power are the collective sum of all generators. If we further assume that all governors and loads are exclusively influenced by the CoI frequency (neglecting the effects of bus frequency deviations and voltage fluctuation), we arrive at the classical Average System Frequency (ASF) model [7]. This is the traditional approach to tackling the second question, i.e., aggregate frequency regulation capacities (active power response) of devices while neglecting the influence of their voltage dynamics. Although CoI and ASF originated in traditional power system, much contemporary research remains fundamentally aligned with their principles. For example, in CIG-integrated power systems, many researchers still consider CoI as the system-wide frequency [8], and integrated the frequency regulations of CIGs into the ASF to assess their impacts [9]–[11]. It is noteworthy that the System Frequency Response (SFR) model and its recent derivatives are also grounded on the ASF [12].

Despite remarkable results have been achieved based on CoI and ASF, they do not provide a rigorous answer for the two questions mentioned earlier, as they have their own assumptions and limitations. Moreover, with the increasing integration of CIGs, the applicability of CoI and ASF will gradually be reduced, as discussed below.

Firstly, it is evident that the CoI frequency does not accurately represent the true system frequency. For instance, in a microgrid comprised entirely of droop-controlled CIGs, we can observe consistency in bus frequencies, indicating the presence of system frequency. However, due to the absence of inertia, it is not possible to calculate the CoI. We note that system frequency lacks a concrete physical entity, which makes it challenging to unveil its fundamental essence.

Secondly, existing system frequency models, such as ASF, are inadequate in considering the voltage dynamics of buses. A substantial body of literature has demonstrated that voltage dynamics can significantly impact system frequency response [13]–[15]. For example, simulation studies of the 9.19 Jinping-Sunan DC lock event found that rapid disconnection of the DC filter capacitor following the incident could raise the frequency nadir from 49.56 Hz to 49.7 Hz, due to decreased voltage level and load power [13]. Ref. [14] assessed the inertia of Nordic power system using measured frequency and power trajectories, revealing that voltage-dependent loads can provide a substantial level of equivalent inertia for the system, e.g., constituting nearly 50% of the total inertia.

Furthermore, numerous recent studies have introduced device control strategies that leverage the interplay of frequency and voltage. For example, [16] used the reactive power control of SGs to provide frequency regulation, leading to a remarkable increase in the frequency nadir. Ref. [8], [17] proposed several integrated frequency-voltage and active-reactive power control method for CIGs, such as the F-Q droop. Similarly, [18] applied a hybrid frequency-voltage control in HVDC to enhance the system stability. These controls intensify the coupling of frequency and voltage, resulting in larger frequency analysis errors when using methods like ASF. It is worth mentioning that a recent concept known as “complex frequency” has emerged, encompassing both voltage and frequency aspects simultaneously. It offers a new interpretation of frequency that takes into account the voltage dynamics [19]. However, this concept is defined at a per-bus level and currently is unclear how to derive the system frequency based on this concept. Overall, the lack of a system frequency model that considers voltage dynamics complicates the frequency stability analysis and may impede the refinement in frequency regulation designs of CIGs.

This paper aims to account for the voltage dynamics in the system frequency analysis from a new perspective. Firstly, we introduce the concept of the Voltage-influenced Common-Mode Frequency (VCMF), as an extension of our previous work Common-Mode Frequency (CMF) [20]. The VCMF is developed by decomposing bus frequencies with non-constant voltages, leveraging the rotational invariance of power flow [21], which is exactly the essence of system frequency. Following the decomposition, the VCMF reflects the influence of voltage dynamics. To be specific, in addition to the *direct frequency-active power (F-P) response* (like inertia, Primary Frequency Control, PFC), voltage dynamics induce an *indirect F-P response*, characterized as “F-Q-V-P”. It is exemplified through test systems involving CIGs equipped with F-Q droop (as proposed in [17]) and nearby Constant Impedance Loads (CILs). When frequency (F) drops, the reactive power (Q) output of CIG decreases, leading to a reduction in load voltage (V) and its active power (P) consumption. On this basis, the main contributions of this work are as follows:

1) The VCMF introduces a new perspective for understanding the system frequency. It shows that the consistency of bus frequencies results from the rotational invariance of power flow rather than inertia-weighted averaging. Thus, VCMF can be employed even in scenarios with zero inertia, where CoI

does not apply.

2) The VCMF analytically describes how voltage dynamics of buses affect the system frequency, leading to significantly improved accuracy in frequency analysis. For example, the VCMF illustrates that the combination of F-Q droop control and nearby CILs is equivalent to F-P droop. This relationship, however, cannot be revealed using tradition methods as ASF.

3) The indirect F-P response in VCMF exhibits globally coupled nature as it involves all devices, making the analysis complicated. Thus, a network partitioning method is proposed, which identifies and cuts off weak paths in the indirect F-P response based on the algebraic connectivity, effectively transforming it from a globally coupling term into several locally coupling terms. It facilitates the calculation and understanding of how voltage affects the system frequency, especially in large-scale power systems.

The rest of this paper is organized as follows: In Section II, the modeling of modern power systems is presented, and some general properties of the systems are introduced for the subsequent derivation. Section III defines the VCMF by decomposing the frequency response, then it is compared with several existing methods. Section IV proposes a network partitioning method using algebraic graph theory. In Section V, the proposed VCMF and network partitioning method are verified through numerical simulations. Finally, conclusions are drawn in Section VI.

Notation: We denote by $\mathbf{0}$ and $\mathbf{1}$ the column vectors or matrices with appropriate dimensions, whose elements are respectively all 0 and 1. We use ω_0 to denote the nominal frequency in rad/s. Given a vector $x = [x_1, \dots, x_n]^T$ or a set of variables x_i , $\text{diag}(x)$ or $\text{diag}(x_i)$ denotes the diagonal matrix whose i -th diagonal element is x_i . We use $\text{triu}(A)$ to denote the upper triangular matrix of A . We use “ s ” to denote the Laplace variable, and “ s ” to denote the diagonal matrix $\text{diag}(s_i)$ with appropriate dimensions. For notational simplicity, “ s ” is omitted if not confusing the understanding.

II. MODELING OF POWER SYSTEMS FOR SYSTEM FREQUENCY ANALYSIS WITH NON-CONSTANT VOLTAGE

This section presents power system models for analyzing the system frequency under non-constant voltage scenarios. In addition, some properties of the generation devices and the transmission network are introduced, which will be utilized in the derivation and simplification of VCMF in Sections III and IV, respectively.

A. Modeling of power systems

Generally, power systems can be conceptualized as multi-input multi-output feedback control systems [22] as depicted in Fig. 1, which can be divided into two parts: generation devices (such as SGs and CIGs) and transmission network. In the following, we will model these two parts separately.

1) *Generation Devices:* The generation devices are represented by Jacobian transfer function matrixes, where the input is the phase angle/voltage amplitude, and the output is the active/reactive power:

$$\begin{bmatrix} \Delta P \\ \Delta Q \end{bmatrix} = - \begin{bmatrix} G_{\theta P}(s) & G_{VP}(s) \\ G_{\theta Q}(s) & G_{VQ}(s) \end{bmatrix} \begin{bmatrix} \Delta \theta \\ \Delta V \end{bmatrix} \quad (1)$$

where Δ denotes the perturbed value of a variable. The vectors ΔP and ΔQ (composed of ΔP_i and ΔQ_i , respectively) represent the active and reactive power outputs of generation devices, where i ranges from 1 to n , with n being the total number of generation devices. Similarly, the vectors $\Delta \theta$ and ΔV (composed of $\Delta \theta_i$ and ΔV_i , respectively) represent phase angles and amplitudes of the device internal voltages, where $\Delta \theta = \omega_0 s^{-1} \Delta \omega$, $\Delta \omega$ is the frequency vector composed of ω_i . The transfer function matrix $G_*(s) = \text{diag}(G_{*,i}(s))$ describes the dynamics of devices, where the subscript $*$ $\in \{\theta P, VP, \theta Q, VQ\}$ denotes the input and output. The negative sign before the transfer function matrix is due to the fact that devices provide positive active and reactive power responses when there is a frequency and voltage drop.

Three types of devices are considered: SGs, Grid-FoLLowing (GFL) converters and Grid-ForMing (GFM) converters [23]. While they have distinct physical characteristics and control schemes, the analysis in this paper is generic and does not depend on these specific characteristics. Therefore, the specific models and Jacobian matrices of the devices are not presented in the main text, for the sake of clarity and readability, but are instead provided in the Appendix.

It is worth noting that loads can be viewed as special devices. Particularly, CILs can also be interpreted as components of the network. We will briefly discuss these two perspectives in the case study. But for the purpose of simplifying the analysis, CILs are predominantly treated as parts of the network, leading to a smaller number of devices.

2) *Transmission Network*: The transmission network is characterized by the power flow equations, which are adequate for the analysis of system frequency, as follows [24], [25]:

$$\begin{bmatrix} \Delta P \\ \Delta Q \end{bmatrix} = - \begin{bmatrix} L_{\theta P} & L_{VP} \\ L_{\theta Q} & L_{VQ} \end{bmatrix} \begin{bmatrix} \Delta \theta \\ \Delta V \end{bmatrix} \quad (2)$$

where L_* is the Jacobin matrix of the network. The explicit expressions of their (diagonal and off-diagonal) elements are

$$\left\{ \begin{array}{l} L_{\theta P}[i, i] = V_i \sum_{j \in i} V_j (-G_{ij} \sin \theta_{ij0} + B_{ij} \cos \theta_{ij0}) \\ L_{\theta P}[i, j] = V_i V_j (G_{ij} \sin \theta_{ij0} - B_{ij} \cos \theta_{ij0}) \\ L_{VP}[i, i] = \sum_{j \in i} V_j (G_{ij} \cos \theta_{ij0} + B_{ij} \sin \theta_{ij0}) + 2V_i G_{ii} \\ L_{VP}[i, j] = V_i (G_{ij} \cos \theta_{ij0} + B_{ij} \sin \theta_{ij0}) \\ L_{\theta Q}[i, i] = V_i \sum_{j \in i} V_j (G_{ij} \cos \theta_{ij0} + B_{ij} \sin \theta_{ij0}) \\ L_{\theta Q}[i, j] = V_i V_j (-G_{ij} \cos \theta_{ij0} - B_{ij} \sin \theta_{ij0}) \\ L_{VQ}[i, i] = \sum_{j \in i} V_j (G_{ij} \sin \theta_{ij0} - B_{ij} \cos \theta_{ij0}) - 2V_i B_{ii} \\ L_{VQ}[i, j] = V_i (-G_{ij} \sin \theta_{ij0} + B_{ij} \sin \theta_{ij0}) \end{array} \right. \quad (3)$$

where $j \in i$ means bus j is adjacent to bus i ; G_{ij} and B_{ij} are elements of the network admittance matrix $Y = G_B + jB_B$, θ_{ij0} is the steady angle difference between bus i and j , and V_{i0} is the steady voltage amplitude of bus i .

3) *Closed-loop System*: As illustrated in Fig. 1, by combining the devices and the network and applying power

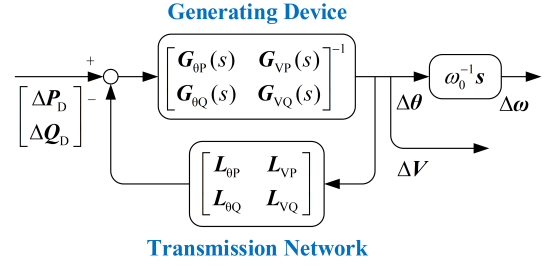


Fig. 1. Closed-loop model for system frequency analysis.

disturbance (ΔP_D and ΔQ_D), the closed-loop response of the system can be expressed as (7), where $H_*(s) = G_*(s) + L_*$.

$$\begin{bmatrix} \Delta \theta \\ \Delta V \end{bmatrix} = \begin{bmatrix} H_{\theta P}(s) & H_{VP}(s) \\ H_{\theta Q}(s) & H_{VQ}(s) \end{bmatrix}^{-1} \begin{bmatrix} \Delta P \\ \Delta Q \end{bmatrix} \quad (4)$$

B. Some general properties of the devices and the network

To facilitate the subsequent derivations in Section III and IV, some properties of the Jacobian matrix of the devices and the network are introduced here.

First, for devices, it is generally observed that $G_{\theta P}(s) \approx 0$ and $G_{\theta Q}(s) \approx 0$ in the low-frequency range. Additionally, devices with good voltage regulation capability, such as SGs and virtual synchronous generators (VSGs), can be effectively modeled as with a large $G_{VQ}(s)$. The reasons are as follows.

1) Based on its physical meaning, we can conclude that $G_{\theta P,i}(s)$ tends to K_{SFC}/ω_0 when s becomes small (K_{SFC} is the gain of secondary frequency control, SFC). Generally, K_{SFC}/ω_0 is either zero or very small, considering that ω_0 is large (314 rad/s or 377 rad/s). 2) As for the $G_{\theta Q}(s)$, if it does not approach zero as s tends to zero, the reactive power output (and thus its voltage) will continue to increase or decrease in the quasi-steady state after frequency dips. Devices are not designed to exhibit such behaviors. 3) A large $G_{VQ}(s)$ indicates that the device can provide significant reactive support with a small voltage dip, enabling it to maintain a nearly constant voltage.

The next property to be introduced is the *rotational invariance of power flow* (with respect to phase angles) [21], which means that the power flow remains the same when the phase angles of all the buses are uniformly increased. Mathematically, it is manifested by the fact that both the network matrices $L_{\theta P}$ and $L_{\theta Q}$ have a right eigenvector of 1 with a corresponding eigenvalue of 1. In other words,

$$L_{\theta P} \mathbf{1} = \mathbf{0}, \quad L_{\theta Q} \mathbf{1} = \mathbf{0} \quad (5)$$

This property serves as the foundation for the derivation of both the CMF and the VCMF. Note that the coherency of bus phase angles corresponds to the coherency of bus frequencies.

Another important property to keep in mind is that large-scale power networks can typically be divided into multiple regions based on the electrical distance, where buses within each region are strongly interconnected while the couplings between regions are relatively weak [26]. Mathematically, this property is reflected in the approximate block diagonal dominance of network Jacobian matrices, indicating that the

magnitudes of entries in the diagonal blocks are relatively larger than those outside the blocks. This property is useful when simplifying the calculation of VCMF, which will be discussed further in Section IV.

III. VOLTAGE-INFLUENCED COMMON-MODE FREQUENCY

This section defines VCMF by decoupling the bus frequencies to extract the common component. A comparison is then made among the VCMF and traditional CoI frequency, ASF, and the previous CMF to showcase its superiority.

A. Derivation of VCMF

In our previous work, the CMF is derived by decomposing bus frequency responses, leveraging the rotational invariance of power flow. However, this method cannot be directly extended to non-constant voltage scenarios, since the invariance of power flow is only with respect to phase angles but not voltages. To tackle this issue, it is crucial to recognize that the incorporation of voltage dynamics aims to achieve a more theoretically rigorous and accurate representation of the system frequency, rather than focusing on the analysis of voltage itself. Thus, voltage variables in (4) can be eliminated via a matrix transformation, as follows:

$$\Delta V = -\mathbf{H}_{VQ}^{-1}(s)\mathbf{H}_{\theta Q}(s)\Delta\theta + \mathbf{H}_{VQ}^{-1}(s)\Delta\mathbf{Q}_D \quad (6)$$

In addition, the frequency response to active and reactive power disturbances can be analyzed separately using the superposition principle. Since active power disturbance dominates frequency response, we will consider this disturbance in the following. Substitute $\Delta\mathbf{Q}_D = \mathbf{0}$ and (6) into (4) yields

$$\Delta\theta = \underbrace{\left(\mathbf{G}_{\theta P}(s) + \mathbf{L}_{\theta P} - \mathbf{H}_{VP}(s)\mathbf{H}_{VQ}^{-1}(s)\mathbf{H}_{\theta Q}(s)\right)^{-1}}_{:=\mathbf{R}^{-1}(s)} \Delta\mathbf{P}_D \quad (7)$$

where $\mathbf{R}^{-1}(s)$ is the closed-loop transfer function between active power disturbance and phase angle response.

Strictly decomposing the phase angle in (7) still remains challenging. In this regard, we propose an approximate decomposition method by using the properties of $\mathbf{R}^{-1}(s)$ in the low-frequency band. For the convenience of discussion, let $\lambda_k(s)$, $\mathbf{u}_k(s)$, and $\mathbf{v}_k(s)$ ($k = 1, \dots, n$) respectively denote the k -th eigenvalue, right and left eigenvector of $\mathbf{R}(s)$, i.e.,

$$\mathbf{R}(s) = \sum_{k=1}^n \lambda_k(s) \mathbf{u}_k(s) \mathbf{v}_k^H(s) \quad (8)$$

Consider that $\mathbf{G}_{\theta P}(s) \approx \mathbf{0}$ and $\mathbf{G}_{\theta Q}(s) \approx \mathbf{0}$ when s is small (as discussed in Section II-B), then $\mathbf{R}(0)$ can be written as

$$\mathbf{R}(0) = \mathbf{L}_{\theta P} - \mathbf{H}_{VP}(0)\mathbf{H}_{VQ}^{-1}(0)\mathbf{L}_{\theta Q} \quad (9)$$

By combining (5) and (9), we can observe that $\mathbf{1}$ is a right eigenvector of $\mathbf{R}(0)$, with eigenvalue 0, i.e., $\lambda_1(0) = 0$, $\mathbf{u}_1(0) = \mathbf{1}$. For the convenience of discussion, we denote by \mathbf{c}/n (a column vector with elements c_i/n) the corresponding left eigenvector $\mathbf{v}_1(0)$, which satisfies $\mathbf{v}_1^T(0)\mathbf{u}_1(0) = 1$.

If we treat $\mathbf{R}(s)$ as the perturbation of $\mathbf{R}(0)$, then according to the matrix perturbation theory [27], $\lambda_1(s)$ can be approximately expressed as

$$\lambda_1(s) \approx \mathbf{v}_1^T(0)\mathbf{R}(s)\mathbf{u}_1(0) \quad (10)$$

By substituting (8) and (9) into (7), and assuming that $\mathbf{u}_1(s) \approx \mathbf{u}_1(0)$, $\mathbf{v}_1(s) \approx \mathbf{v}_1(0)$, then we can approximately obtain one component of $\Delta\theta$, whose differentiation is

$$\begin{cases} \Delta\omega_{\text{VCM}}(s) = \frac{s\omega_0^{-1}\mathbf{c}^T\Delta\mathbf{P}_D(s)}{\sum_{i=1}^n c_i G_{\theta P,i}(s) + \text{VCT}} \mathbf{1} \\ \text{VCT} := -\mathbf{c}^T \mathbf{H}_{VP}(s) \mathbf{H}_{VQ}^{-1}(s) \mathbf{H}_{\theta Q}(s) \mathbf{1} \end{cases} \quad (11)$$

This frequency component is consistent across all the buses, which is defined as the ‘‘VCMF’’ in this paper. It can be inferred from the derivation that the consistency is a result of the rotational invariance of power flow, rather than being attributed to inertia-weighted averaging. It is also worth mentioning that c_i can represent the weighting of each bus, similar to CMF.

The VCMF encompasses both the direct F-P response ($G_{\theta P,i}(s)$), as well as the indirect one, i.e., the second term in the denominator, where the reactive power/voltage responses of all devices are coupled through the network, following the action path of F-Q-V-P. If all bus voltages are maintained constant, this term becomes zero and is hence referred to as the Voltage Coupling Term (VCT). In traditional controls, reactive power/voltage are typically independent of frequency. However, recent advancements in CIG controls have introduced complex couplings between frequency and reactive power/voltage [16]–[18]. When combined with voltage-dependent loads, e.g., CILs, the F-Q-V-P pathway is activated. In such scenarios, relying solely on the direct F-P response is inadequate for accurately analyzing system frequency.

The derivation of VCMF relies on some approximations, e.g., we assume $\mathbf{u}_1(s) \approx \mathbf{u}_1(0) = \mathbf{1}$, $\mathbf{v}_1(s) \approx \mathbf{v}_1(0)$. They are valid in the low-frequency range as discussed in Section II-B, where dynamics of the system frequency mainly belong to. Case studies show that with these approximations, VCMF can persistently represent the system frequency.

In the presence of SFC, $\mathbf{G}_{\theta P}(0) \neq \mathbf{0}$, there might be discrepancies between $\mathbf{u}_1(0)$ and $\mathbf{1}$, resulting in variations in the VCMF across buses. In fact, it aligns with physical intuition. For example, when frequency gradually recover after a disturbance, devices equipped with SFC experience a continuous increase in active power output. Consequently, their phase angle differences with other devices (not equipped with SFC) also grow, leading to disparities in bus frequencies. We note that these differences are typically very small, as demonstrated in the case study in Section V-B.

B. Comparison of VCMF with existing methods

For a comprehensive understanding, the VCMF is compared with existing system frequency define/representation methods (CoI frequency) and frequency analysis models (ASF). TABLE I summarizes the comparisons.

1) System frequency define/representation methods

The CoI frequency is the most widely accepted method for defining/representing system frequency. However, it lacks a rigorous theoretical foundation and is essentially heuristic. For example, it cannot account for the concept of system frequency in zero-inertia power systems.

Compared to CoI frequency, CMF/VCMF is obtained by decoupling bus frequencies based on the rotational invariance

TABLE I
COMPARISON OF REPRESENTATIONS AND ANALYTICAL MODELS OF SYSTEM FREQUENCY

	CoI	ASF	CMF	VCMF
Theoretical foundation	Heuristic	Averaging of bus frequencies	Decoupling of bus frequencies ($\Delta \mathbf{V} = \mathbf{0}$)	Decoupling of bus frequencies ($\Delta \mathbf{V} \neq \mathbf{0}$)
Expression	$\Delta \omega_{\text{CoI}} = \frac{\mathbf{J}^T \Delta \omega}{\mathbf{J}^T \mathbf{1}}$	$\Delta \omega_{\text{AS}} = \frac{s \omega_0^{-1} \mathbf{1}^T \Delta \mathbf{P}_D}{\sum G_{\theta P,i}(s)}$	$\Delta \omega_{\text{CM}} = \frac{s \omega_0^{-1} \mathbf{c}^T \Delta \mathbf{P}_D}{\sum c_i G_{\theta P,i}(s)}$	$\Delta \omega_{\text{CM}} = \frac{s \omega_0^{-1} \mathbf{c}^T \Delta \mathbf{P}_D}{\sum c_i G_{\theta P,i}(s) + \text{VCT}}$
Suit for zero-inertia system?	No	Yes	Yes	Yes
Could analyze bus weighting?	-	No	Yes	Yes
Could analyze voltage impact?	-	No	No	Yes

of power flow. Thus, they are more theoretically rigorous and more applicable, e.g., for zero-inertia systems.

We acknowledge that there are alternative frequency definitions, like “complex frequency” [19]. However, complex frequency is defined for individual buses, which is not in the scope of this paper (i.e., analyzing system frequency).

2) System frequency analysis models

The ASF is a traditional system frequency analysis model, whose basic idea is to represent CoI frequency [7]. Its derivation relies on certain assumptions, including constant voltages, which may lead to inaccuracies in the analysis. Strictly speaking, the ASF will lose its theoretical basis in zero-inertia systems due to its derivation is dependent on CoI. Nevertheless, the ASF expression itself does not directly correlate with CoI. As a result, it can still find application in zero-inertia systems, albeit as a pragmatic approach.

The CMF and VCMF are based on decomposition rather than CoI, thus they are more theoretically rigorous. We note that VCMF is consistent with CMF if the voltage is constant. In such cases, the VCT is zero and the weighing coefficients c_i of CMF and VCMF are both determined by $\mathbf{L}_{\theta P}$. If the network is further lossless (no CILs), their expressions will be the same as ASF, since $c_i = 1$ in this case [20].

In summary, VCMF is more theoretically rigorous than CoI frequency and ASF. It can be viewed as the extension of ASF and CMF. The consideration of the VCT allows for the analysis of voltage impact, which makes the VCMF more accurate and comprehensive.

However, the VCT couples the dynamics of all devices, making it challenge to analyze. To solve this problem, the next section gives a method to decompose the VCT into several low-order terms, which helps to simplify the analysis and understand the impacts of voltage on the system frequency.

IV. DECOUPLING OF VOLTAGE COUPLING TERM

This section approximately decomposes the VCT into several terms based on the block diagonal property of the network matrix, which simplifies the analysis of VCMF.

A. Decoupling method of the VCT

For the sake of clarity, the VCT in (11) is rewritten as:

$$\begin{aligned}
 & -\mathbf{c}^T \mathbf{H}_{VP}(s) \mathbf{H}_{VQ}^{-1}(s) \mathbf{H}_{\theta Q}(s) \mathbf{1} = \\
 & -\underbrace{\mathbf{c}^T (\mathbf{G}_{VP}(s) + \mathbf{L}_{VP})}_{\text{row}} \cdot \underbrace{(\mathbf{G}_{VQ}(s) + \mathbf{L}_{VQ})}_{\text{square}} \cdot \underbrace{\mathbf{G}_{\theta Q}(s) \mathbf{1}}_{\text{column}}
 \end{aligned} \quad (12)$$

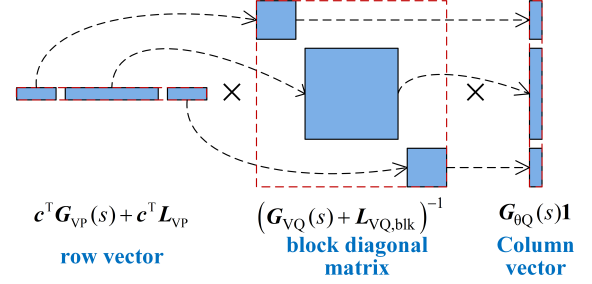


Fig. 2. Schematic diagram of the decoupling of VCT.

where $\mathbf{L}_{\theta Q} \mathbf{1} = \mathbf{0}$ is used.

The above equation shows that the VCT is computed by multiplying three parts: a row vector, a square matrix, and a column vector. The i -th element of the row vector/column vector is only related to the i -th device. But the elements in the inverse of the middle square matrix may be relevant to almost all the devices in the system, due to the fact that \mathbf{L}_{VQ} is typically full (passive buses are reduced). Thus, it can be concluded that the inverse of the middle matrix introduces the coupling among all the devices, and the key to simplifying the VCT is to simplify the \mathbf{L}_{VQ} matrix.

As analyzed in Section II-B, the matrix \mathbf{L}_{VQ} is generally block diagonally dominated. If the elements in the off-diagonal block can be ignored, then the VCT is approximately decomposed into several terms, and each term is only related to the devices in each block, as illustrated in Fig. 2. We note that the simplification of \mathbf{L}_{VQ} can be interpreted as cut off some weak Q-V path in the F-Q-V-P response. It transforms the VCT from globally coupling to locally coupling, which simplifies the analysis of VCT and VCMF.

Suppose that the power system is already partitioned into m regions (how to partition will be discussed in the next subsection), and denote the simplified \mathbf{L}_{VQ} matrix by $\mathbf{L}_{VQ,blk}$, then the approximate VCMF (xVCMF) can be expressed as:

$$\Delta \omega_{\text{xVCM}}(s) = \frac{s \omega_0^{-1} \mathbf{c}^T \Delta \mathbf{P}_D(s)}{\sum_{i=1}^n c_i G_{\theta P,i}(s) - \sum_{i=1}^m \mathbf{H}_{VP,blk,i} \mathbf{H}_{VQ,blk,i}^{-1} \mathbf{H}_{\theta Q,blk,i}} \quad (13)$$

where $\mathbf{H}_{VP,blk,i}$, $\mathbf{H}_{\theta Q,blk,i}$ and $\mathbf{H}_{VQ,blk,i}$ are respectively the i -th sub-vector/diagonal block of \mathbf{H}_{VP} , $\mathbf{H}_{\theta Q}$ and \mathbf{H}_{VQ} . The “s” is omitted for notational simplicity.

B. Partitioning of the network

Power system partitioning is a widely studied problem, and there are many well-established methods [28], [29]. For the concern of this paper, the partitioning problem can be described as the following optimization problem

$$\begin{aligned} \min_{e \in E} \quad & \delta \\ \text{s.t.} \quad & \max_i \text{size}(\mathbf{L}_{VQ, \text{blk}, i}) \leq N_{\max} \end{aligned} \quad (14)$$

where E denotes the set of all partitioning strategies and e is one of them. The notation $\text{size}(\mathbf{A})$ denotes the number of rows of matrix \mathbf{A} . The constraint ensures the number of devices in each block is not greater than the allowed value N_{\max} , which makes the calculation and analysis of VCMF simple enough. The choice of N_{\max} depends on the desired calculation burden. A larger N_{\max} yields more accurate results but also increases the computational complexity. It should be noted that if the devices are reasonably aggregated firstly (e.g., aggregating wind turbines in a wind farm), the N_{\max} can be significantly reduced while achieving the same accuracy. δ denotes the relative error of the middle matrix in VCT and its simplification, as in (15). Minimizing δ ensures the xVCMF is as accurate as possible.

$$\delta = \frac{\|(\mathbf{G}_{VQ}(s) + \mathbf{L}_{VQ})^{-1} - (\mathbf{G}_{VQ}(s) + \mathbf{L}_{VQ, \text{blk}})^{-1}\|}{\|(\mathbf{G}_{VQ}(s) + \mathbf{L}_{VQ, \text{blk}})^{-1}\|} \quad (15)$$

where $\|\mathbf{A}\|$ denotes the matrix norm of \mathbf{A} , e.g., \mathcal{H}_∞ norm.

The optimization problem (14) is combinatorial and computationally hard, considering the number of possible partitioning strategies is huge. Here we propose a method to obtain the suboptimal solution based on algebraic graph theory.

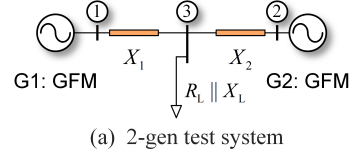
Given a Laplacian matrix of a graph, the second-smallest eigenvalue, known as the algebraic connectivity, is a measure that provides insights into the connectivity and structure of the graph [30]. Smaller algebraic connectivity indicates a stronger separation between two subgraphs, i.e., with fewer edges (or their weightings are smaller) connecting the two parts. Additionally, the sign of the elements in the corresponding eigenvector can be used to distinguish the two subgraphs [31].

To minimize δ , it is crucial to carefully select the small off-diagonal elements of \mathbf{L}_{VQ} (weak V-Q connection in the system) to be neglected. In this regard, a Laplacian matrix can be formulated based on \mathbf{L}_{VQ} to identify these weak couplings. Thus, a suboptimal yet effective solution to the optimization problem (17) can be obtained as follows.

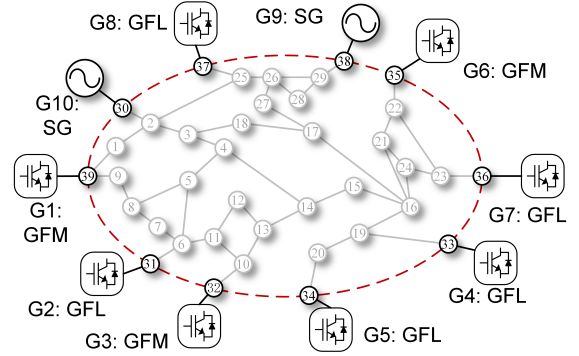
1) Define Laplacian matrix $\mathbf{L}_{VQ, L} = \text{triu}(\mathbf{L}_{VQ}) + \text{triu}(\mathbf{L}_{VQ})^T - \text{diag}((\text{triu}(\mathbf{L}_{VQ}) + \text{triu}(\mathbf{L}_{VQ})^T)\mathbf{1})$, which is a Laplacian constructed based on the upper triangle of \mathbf{L}_{VQ} . Note that \mathbf{L}_{VQ} exhibits near symmetry, making use of either its upper or lower triangle equivalent. Then partitioning the power system (\mathbf{L}_{VQ}) into two regions (two diagonal-block) according to the algebraic connectivity and corresponding eigenvector of $\mathbf{L}_{VQ, L}$.

2) For each region, if the number of containing devices exceeds the given N_{\max} , partition the region into two subregions similar to step 1.

3) Repeat step 2 iteratively until the number of devices in all regions is not greater than N_{\max} .



(a) 2-gen test system



(b) 10-gen test system

Fig. 3. (a) 2-gen test system, (b) 10-gen test system.

The proposed method significantly reduces the computational complexity compared to an exhaustive search, making it applicable to large-scale power systems. Then xVCMF can be calculated and analyzed easily.

V. CASE STUDY

In this section, the effectiveness of VCMF and xVCMF are validated via numerical simulations using MATLAB/Simulink. While the analysis is linearized, the simulations are conducted with high-fidelity and nonlinear models.

A. Test system descriptions

Two test systems are utilized in case studies, illustrated in Fig. 3. The power base value for both systems is 600 MVA, and the nominal frequency is 60 Hz. There are three types of generation devices, i.e., SGs, GFL and GFM converters. The GFL converters are equipped with F-P and F-Q droop [17], with gain D_{GFL} and K_{FQ} respectively. The GFM operates as a VSG, with virtual inertia J_{GFM} and damping coefficient D_{GFM} . Models and main parameters of these devices can be founded in Appendix-A, unless otherwise specified.

The 2-gen system is employed to illustrate the influence of voltage dynamics on frequency and the validity of VCMF. It briefly explores the difference between treating CILs as network or devices (in the latter case, the system consists of 3 devices). Additionally, it demonstrates the influence of SRC. The system comprises a GFL converter, a GFM converter and a CIL. The parameters of the load and transmission lines are $R_L = 1$ pu, $X_L = 8$ pu, and $X_1 = X_2 = 0.2$ pu.

The 10-gen system is utilized to further demonstrate the applicability of VCMF and its simplification xVCMF in larger-scale power systems. The test system consists of 5 GFL converters, 3 GFM converters and 2 SGs. Loads locate at bus 15, 16, 18, 21, 24, 26, 27 and 28 (same as [20]), collectively consume approximately 8 pu active power and 1 pu reactive power. The network parameters are identical to the IEEE standard 39-bus system [32].

TABLE II
WEIGHTING VECTORS OF TEST SYSTEMS

Test system	weighting coefficients				
2-gen	$c_1 = 0.983$ (load as a part of network)	$c_2 = 1.017$	$c_1^{(3)} = 1.000$ (load as a device)	$c_2^{(3)} = 1.036$	$c_3^{(3)} = 0.964$
10-gen	$c_1 = 1.001$ $c_6 = 0.966$	$c_2 = 1.053$ $c_7 = 0.965$	$c_3 = 1.059$ $c_8 = 1.080$	$c_4 = 1.030$ $c_9 = 0.826$	$c_5 = 1.020$ $c_{10} = 1.000$

TABLE III
COMPARISON OF QUASI-STEADY-STATE FREQUENCY OBTAINED BY SIMULATIONS AND THEORETICAL ANALYSES

	K_{FQ}/pu	Simu/Hz	ASF/Hz	CMF/Hz	VCMF/Hz
2-gen	0	-0.587	-0.600 (2.3%)	-0.590 (0.5%)	-0.590 (0.5%)
	-20	-0.435	-0.600 (38.0%)	-0.590 (35.6%)	-0.441 (1.5%)
	-40	-0.342	-0.600 (75.3%)	-0.590 (72.2%)	-0.353 (3.0%)
	K_{FQ}/pu	Simu/Hz	ASF/Hz	xVCMF/Hz	VCMF/Hz
10-gen	0	-0.214	-0.250 (16.8%)	-0.221 (3.2%)	-0.221 (3.2%)
	-20	-0.177	-0.250 (24.5%)	-0.187 (5.8%)	-0.184 (4.2%)
	-40	-0.150	-0.250 (66.3%)	-0.162 (8.1%)	-0.158 (5.3%)

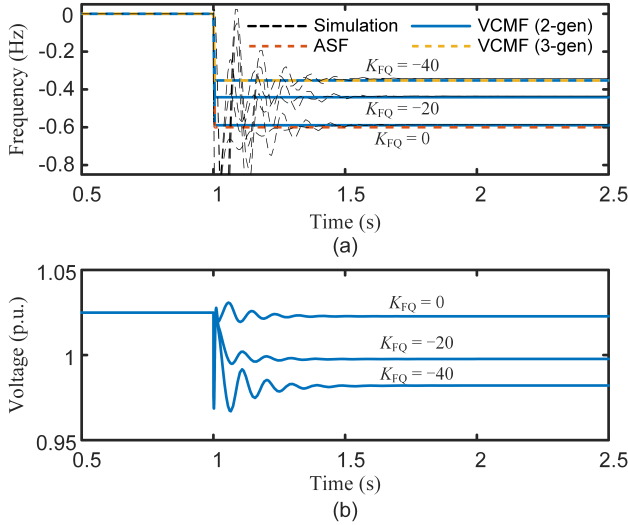


Fig. 4. Time-domain simulation and theoretical results in the 2-gen system. (a) Comparison of the frequency trajectories obtained by simulations, ASF and VCMF. (b) Trajectories of load voltage.

TABLE II presents the weighting coefficients of the two systems according to (9).

B. Case Studies on the 2-gen Test System

In the 2-gen system, the virtual inertia of the CIGs is set to 0, resulting in a zero-inertia system. Thus, the CoI frequency does not apply in this system.

Considering a power step of 0.2 pu in G1 ($\Delta P_{D,1}(s) = -0.2/s$), Fig. 4 (a) depicts the bus frequency trajectories for different K_{FQ} . As K_{FQ} increases, the frequencies show a significant rise, which can be explained by Fig. 4 (b). When the frequency drops, the negative F-Q droop gain causes the

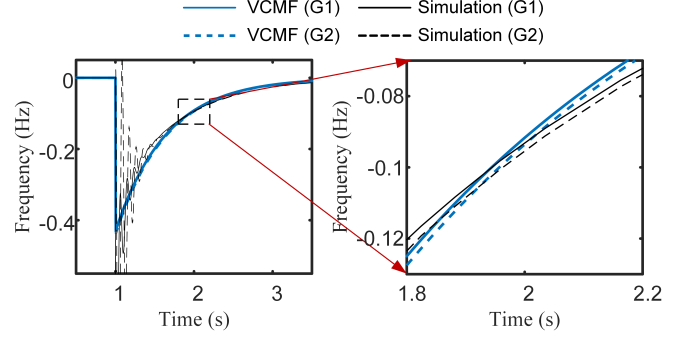


Fig. 5. Time-domain simulation and theoretical results in the 2-gen system when SFC exists.

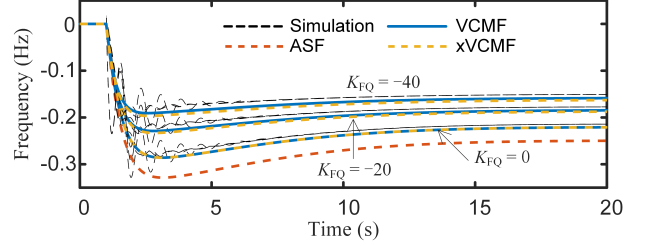


Fig. 6. Frequency trajectories obtained by time-domain simulations and theoretical analyses in the 10-gen system.

converter to output less reactive power. Consequently, the load voltage and active power consumption decrease, resulting in a reduction in the frequency drop.

According to (11) and TABLE I, the VCMF and ASF in this system is as follows (CMF is the same as VCMF in the case of $K_{FQ} = 0$).

$$\begin{aligned} \Delta\omega_{VCM} &= \frac{c_1 \Delta P_{D1}(s)}{c_1 D_{GFM} + c_2 D_{GFL} - \frac{(c_1 L_{VP,12} + c_2 L_{VP,22}) K_{FQ}}{L_{VQ,22}}} \\ &= \frac{c_1 \Delta P_{D1}(s)}{c_1 D_{GFM} + c_2 D_{GFL} - 0.336 K_{FQ}} \end{aligned} \quad (16)$$

$$\Delta\omega_{AS} = \frac{\Delta P_{D1}(s)}{D_{GFM} + D_{GFL}} \quad (17)$$

It can be inferred from (16) that the F-Q droop has a similar effect to the F-P droop. Its effect is influenced by network structure, parameters (including reduced load) and the value of K_{FQ} . When $K_{FQ} = -20$ pu or -40 pu, the equivalent frequency damping is respectively 6.72 pu and 13.44 pu, which is comparable to the damping provided by converters.

Fig. 4 (a) also shows the VCMF, CMF and ASF obtained by (16) and (17). TABLE III provides the error analysis, where the simulation results serve as the reference. Notably, the relative errors of the ASF and CMF can reach up to 70%, whereas that of VCMF remains below 5%. These results demonstrate the influence of voltage dynamics and the efficacy of VCMF.

The VCMF can also be calculated if the CIL is viewed as a device, as in (18), where the superscript “(3)” denotes 3-gen. It can be clearly observed that the equivalent damping is mainly the result of the combination of F-Q droop and CIL load. If the numerator and denominator in (16) and (18) are divided by c_1 or $c_1^{(3)}$ at the same time, respectively, the two results are

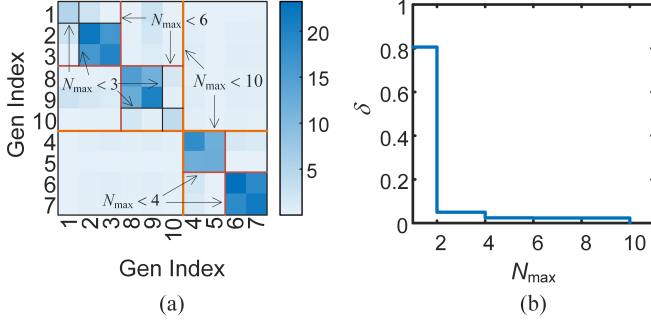


Fig. 7. Partitioning results for different N_{\max} . (a) The heatmap of L_{VQ} with split lines, where the order of devices is readjusted. (b) relative error δ .

exactly the same, which is verified in Fig. 4 (a) (taking the case of $K_{FQ} = -40$ pu as an example). Because considering loads as parts of the network can significantly reduce the number of devices, we will adopt this perspective in the next test system.

$$\Delta\omega_{VCM}^{(3)} = \frac{c_1^{(3)} \Delta P_{D1}(s)}{c_1^{(3)} D_{GFM} + c_2^{(3)} D_{GFL} - (0.021 + 0.321 R_L^{-1}) K_{FQ}} \quad (18)$$

To illustrate the impact of SFC on VCMF, we set the K_{SFC} of G1 (GFM) to be 40 pu in the case of $K_{FQ} = -20$ pu. This results in $\mathbf{u}_1(0) = [0.99, 1.01]^T$, deviating slightly from 1. It means that the VCMF trajectory of G1 is 0.98 times that of G2, which is confirmed by simulation results in Fig. 5. Notably, even with a relatively large SFC gain in this case, the difference between $\mathbf{u}_1(0)$ and 1 remains quite small. This implies that this difference is typically negligible in practice.

C. Case Studies on the 10-gen Test System

In the 10-gen system, considering a power step disturbance of 0.5 pu occurring in G9, Fig. 5 presents the VCMF and bus frequency trajectories obtained by simulations. The corresponding relative errors are also provided in TABLE III. It can be observed that as the system scale and complexity increase, the errors of VCMF slightly increase compared to the previous test system, but it remains significantly more accurate than ASF. Notably, even when $K_{FQ} = 0$, ASF differs considerably from the simulation results, due to the assumption of equal weightings for each bus. However, c_9 is only 0.826, indicating that the impact of the disturbance located at G9 is 17.4% less significant than suggested by ASF.

Next, we verify the effectiveness of the network partitioning method and xVCMF. Fig. 7 gives the partitioning results and the relative error δ (by (15)) for different N_{\max} . Each pair of split lines in Fig. 7 (a) correspond to a step of δ in Fig. 7 (b). For instance, when N_{\max} is set to 10, there is no need for partitioning, and the δ is zero. When $N_{\max} \in [6, 9]$, the network will be divided into two regions, i.e., G1-G3, G8-G10 and G4-G7, and δ rises to 2.3%.

It can be observed from Fig. 7 (a) that most off-diagonal elements in L_{VQ} matrix is very small, which allows the proposed partitioning method to effectively separate the power network while preserving main couplings. Even when N_{\max} is set to 2, the relative error δ is only 5.0%. Thus, we choose

TABLE IV
EQUIVALENT FREQUENCY DAMPING OF EACH REGION PROVIDED BY F-Q DROOP (PU VALUES)

N_{\max}	G1	G2	G3	G8	G9	G10	G4	G5	G6	G7	Sum
1	0	1.67	0	2.74	0	0	17.43	1.01	0	2.80	25.64
2	0	1.67		2.74	0		36.12			2.80	43.32
3		1.67			2.74		36.12			2.80	43.32
4-5		1.67			2.74			41.02			45.42
6-9				4.45				41.02			45.47
10						47.08					47.08

$N_{\max} = 2$ to calculate the xVCMF. The xVCMF is compared to VCMF in Fig.6 and TABLE III. The results illustrate that xVCMF closely approximates VCMF and is significantly more accurate than ASF, even in the case of $K_{FQ} = -40$ pu.

For a comprehensive understanding, TABLE IV shows the equivalent frequency damping provided by F-Q droop in each partitioned region, considering the case of $K_{FQ} = -40$ pu. It can be observed that although all GFL converters share the same K_{FQ} , the damping values of each converter (or region) vary significantly. This discrepancy is closely related to the distribution of converters and loads within the system. Additionally, the sum of damping across all regions is found to be monotonically non-decreasing as N_{\max} increases. Notably, when $N_{\max} = 2$, the sum of damping is very close to that obtained when $N_{\max} = 10$. This further validates the effectiveness of the network partitioning method the xVCMF.

Combining the case studies in this section, it can be concluded that the proposed VCMF is suitable for representing system frequency even in the scenario of zero-inertia, where CoI frequency cannot be calculated. Besides, when voltage dynamics play a significant role, the VCMF proves to be highly effective in accurately characterizing the system frequency responses. In contrast, ASF and earlier CMF exhibit notable deviations from the system frequency. Additionally, the partitioning of the network in large-scale power systems can be achieved by selectively ignoring certain non-diagonal elements of the L_{VQ} matrix, based on the algebraic connectivity of the constructed Laplacian matrix. This partitioning approach greatly facilitates the calculation and analysis of VCMF.

VI. CONCLUSIONS AND DISCUSSIONS

Various novel control strategies of CIGs intensify the coupling between frequency and voltage in power systems, leading to a reduced applicability of traditional frequency analysis methods. To this end, this paper defined VCMF to understand and analyze the system frequency when impacts of voltage dynamics cannot be ignored. It has been demonstrated that:

1) The VCMF offers an improved understanding of system frequency compared to CoI. It demonstrates that the system frequency is not be an inertia-weighted average but rather a common component of the bus frequencies, which stems from the rotational invariance of power flow. This new perspective allows for understanding the system frequency even in zero-inertia systems.

2) By incorporating the indirect F-P responses caused by voltage dynamics, VCMF provides a more precise and com-

TABLE V
MAIN PARAMETERS OF GENERATION DEVICES (PU VALUE)

$J_{SG} = 10$	$D_{SG} = 0$	$K_{SG} = 20$	$K_1 = 0.22$	$K_3 = 0.22$
$K_5 = 0.3$	$K_7 = 0.26$	$T_1 = 0.2$	$T_2 = 0$	$T_3 = 0.1$
$T_4 = 0.25$	$T_5 = 4$	$T_6 = 4$	$T_7 = 0.4$	$D_{GFL} = 10$
$J_{GFM} = 10$	$D_{GFM} = 10$			

prehensive characterization of the system frequency behaviors, compared to ASF and CMF. This is demonstrated through test systems where converters are equipped with F-Q droop. Simulation results indicate that VCMF significantly reduces the error in determining the frequency response (reducing the error from up to 60%-70% to approximately 5%).

3) Analyzing VCMF in large-scale power systems can be challenging due to the complexity and computational burden associated with the globally coupling term. To address this, a network partitioning method is proposed based on the algebraic connectivity of the constructed $L_{VQ,L}$ matrix. This method selectively neglects the small non-diagonal elements in the network matrix, effectively cutting the weak Q-V path, decomposing the globally coupling term into several locally coupling terms. The resulting xVCMF exhibits similar behaviors to the original VCMF, but is much easier to analyze.

We acknowledge that the analysis of VCMF is more complex compared to existing methods, such as ASF. For example, VCMF requires power flow information (for weighting vector c) and the voltage response models of devices. However, it is essential to emphasize that VCMF provides a way for integrating these factors into the system frequency model, while tradition methods cannot accommodate them. When this information is lacking, VCMF is not rendered inapplicable. If voltage response models of certain devices are unavailable, a rough approximation is to assume them have constant voltages. Besides, if power flow data is unavailable, we can simplify the VCMF by setting the weighting vector c to zero. Notably, in these scenarios, the analysis accuracy of the VCMF will not be lower than traditional methods.

The analysis of VCMF is under the assumption of linearization, which may be necessary considering the complexity of large-scale nonlinear systems. There are some practical methods for addressing the nonlinearity, e.g., replace the transfer functions $G_{\theta P,i}(s)$ with nonlinear models [20]. We note that it is possible to rigorously extend VCMF to the nonlinear case, considering that the foundation of VCMF, namely the rotational invariance of power flow, still holds in the nonlinear case. We consider this as a future direction.

APPENDIX A

MODELS OF GENERATION DEVICES AND LOADS

Models of the SG, GFL and GFM converter used in simulations are shown in Fig. 8. Loads are CILs, i.e., parallel resistance R_L and reactance X_L . In Fig. 8 (b), the F-P and F-Q droop can be expressed as (19), where D_{GFL} and K_{FQ} are respectively the gains.

$$\begin{cases} P^{\text{ref}} = P_0 - D_{GFL}(\omega_{\text{PLL}} - 1) \\ Q^{\text{ref}} = Q_0 - K_{FQ}(\omega_{\text{PLL}} - 1) \end{cases} \quad (19)$$

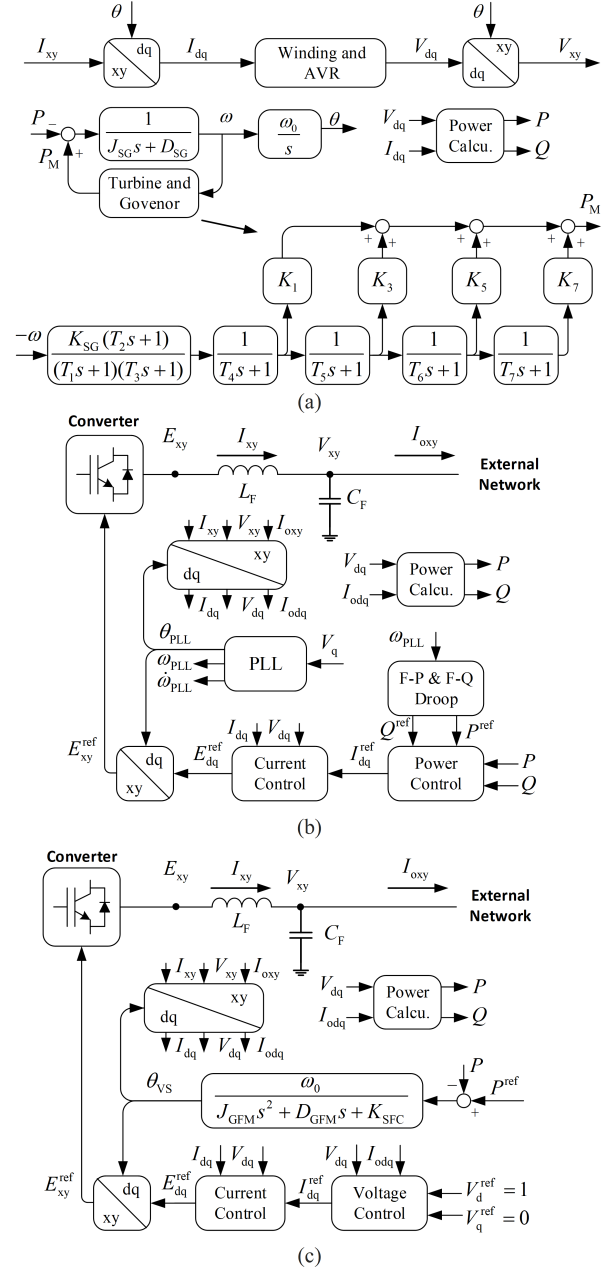


Fig. 8. Models of (a) SG, (b) GFL converter and (c) GFM converter.

Main parameters of these three types of generation devices are given in TABLE V. Due to page limits, we do not give the detailed explanation of the models, as well as the parameters, they can be referred to [23], [33], [34].

APPENDIX B

SIMPLIFIED JACOBINE TRANSFER FUNCTION MATRIXES

The accurate Jacobian matrices based on above models are typical of a high order, which poses challenges in the calculation of VCMF. For instance, it is difficult to precisely obtain the expression of the inverse of $(G_{VQ}(s) + L_{VQ})$. Thus, simplified Jacobian matrices are employed in theoretical

analysis, as follows:

$$\left\{ \begin{array}{l} \text{(SG)} \quad \begin{bmatrix} s\omega_0^{-1}(J_{SG}s + D_{SG} + G_T(s)) & 0 \\ 0 & \eta \end{bmatrix} \\ \text{(GFL)} \quad \begin{bmatrix} s\omega_0^{-1}D_{GFL} & 0 \\ s\omega_0^{-1}K_{FQ} & 0 \end{bmatrix} \\ \text{(GFM)} \quad \begin{bmatrix} s\omega_0^{-1}(J_{GFM}s + D_{GFM} + s^{-1}K_{SFC}) & 0 \\ 0 & \eta \end{bmatrix} \\ \text{(CIL)} \quad \begin{bmatrix} 0 & 2V_0R_L^{-1} \\ 0 & 2V_0X_L^{-1} \end{bmatrix} \end{array} \right. \quad (20)$$

where $G_T(s)$ is the transfer function of turbine and governor, as shown in Fig. 8 (a); η is a large number, such as 1×10^6 .

The above simplification is justified by the following reasons: for SGs and GFMs, they can maintain nearly constant voltages, allowing them to be approximated with a high gain in the voltage-reactive power (V-Q) loop, as discussed in Section II-B. For GFL and GFM converters, their power regulation dynamics are typically fast. In this case, the F-P and F-Q loops can be accurately characterized by parameters such as D_{GFL} and K_{FQ} .

We note that these simplifications may not suit all devices, e.g., where control delays of CIGs cannot be ignored. However, the primary focus of this paper is to address the recognition and calculation of system frequency in the scenario of non-constant voltages, and these models are considered sufficient to demonstrate the effectiveness of the proposed VCMF. Dealing with more complex models and achieving more accurate calculations using high-order models will be the subject of future research.

REFERENCES

- [1] F. Milano, F. Dörfler, G. Hug, D. J. Hill, and G. Verbič, "Foundations and challenges of low-inertia systems," in *2018 power systems computation conference (PSCC)*. IEEE, 2018, pp. 1–25.
- [2] "Technical report on the events of 9 august 2019," National Grid ESO, Tech. Rep., 2019.
- [3] B. Magnus, "Review of feb. 2021 extreme cold weather event-ercot presentation," ERCOT, Tech. Rep., 2021.
- [4] N. Hatziaargyriou, J. Milanovic, C. Rahmann, V. Ajjarapu, C. Canizares, I. Erlich, D. Hill, I. Hiskens, I. Kamwa, B. Pal *et al.*, "Definition and classification of power system stability-revisited & extended," *IEEE Trans. Power Systems*, vol. 36, no. 4, pp. 3271–3281, 2020.
- [5] M. Wang, J. Guo, S. Ma, T. Wang, X. Zhang, K. Luo, and W. Guozheng, "Review of transient frequency stability analysis and frequency regulation control methods for renewable power systems," *Proc. CSEE*, vol. 43, no. 05, pp. 1672–1694, 2023.
- [6] Z. Han, P. Ju, C. Qin, D. Sun, H. Sun, and Y. Zheng, "Review and prospect of research on frequency security of new power system," *Autom. Elect. Power Syst.*, 2023.
- [7] M. L. Chan, R. Dunlop, and F. Schweppe, "Dynamic equivalents for average system frequency behavior following major disturbances," *IEEE Trans. Power Appar. Syst.*, no. 4, pp. 1637–1642, 1972.
- [8] F. Milano, B. Alhanjari, and G. Tzounas, "Enhancing frequency control through rate of change of voltage feedback," *IEEE Trans. Power Syst.*, 2023.
- [9] C. Zhao, D. Sun, X. Zhang, W. Ke, B. Hu, and H. Nian, "A two-stage power distribution scheme of multiple wind farms participating in primary frequency regulation," *IEEE Trans. Power Syst.*, 2022.
- [10] Z. Shi, Y. Xu, Y. Wang, J. He, G. Li, and Z. Liu, "Coordinating multiple resources for emergency frequency control in the energy receiving-end power system with hvdc," *IEEE Trans. Power Syst.*, 2022.
- [11] X. Tang, Y. Li, M. Yang, Y. Wu, and Y. Wen, "Adaptive event-triggered model predictive load frequency control for power systems," *IEEE Trans. Power Syst.*, 2022.
- [12] P. Ju, Y. Zheng, Y. Jin, C. Qin, Y. Jiang, and L. Cao, "Analytic assessment of the power system frequency security," *IET Gener. Transm. Distrib.*, vol. 15, no. 15, pp. 2215–2225, 2021.
- [13] Z. Li, X. Wu, K. Zhuang, L. Wang, Y. Miao, and B. Li, "Analysis and reflection on frequency characteristics of east china grid after bipolar locking of "9.19" jinping-sunan dc transmission line," *Automation of Electric Power Systems*, vol. 41, no. 7, pp. 149–155, 2017.
- [14] D. Wilson, J. Yu, N. Al-Ashwal, B. Heimisson, and V. Terzija, "Measuring effective area inertia to determine fast-acting frequency response requirements," *International Journal of Electrical Power & Energy Systems*, vol. 113, pp. 1–8, 2019.
- [15] H. Sun, B. Wang, W. Li, C. Yang, W. Wei, and B. Zhao, "Research on inertia system of frequency response for power system with high penetration electronics," *Proc. CSEE*, vol. 40, no. 16, pp. 5179–5191, 2020.
- [16] A. Moeini and I. Kamwa, "Analytical concepts for reactive power based primary frequency control in power systems," *IEEE Trans. Power Syst.*, vol. 31, no. 6, pp. 4217–4230, 2016.
- [17] W. Zhong, G. Tzounas, and F. Milano, "Improving the power system dynamic response through a combined voltage-frequency control of distributed energy resources," *IEEE Trans. Power Syst.*, vol. 37, no. 6, pp. 4375–4384, 2022.
- [18] M. Gu, L. Meegahapola, and K. L. Wong, "Coordinated voltage and frequency control in hybrid ac/mt-hvdc power grids for stability improvement," *IEEE Trans. Power Syst.*, vol. 36, no. 1, pp. 635–647, 2020.
- [19] F. Milano, "Complex frequency," *IEEE Trans. Power Syst.*, vol. 37, no. 2, pp. 1230–1240, 2021.
- [20] H. Gao, H. Xin, L. Huang, Z. Li, W. Huang, C. Wu, and P. Ju, "Common-mode frequency in converter-integrated power systems: Definition, analysis, and quantitative evaluation," *IEEE Trans. Power Syst.*, vol. 37, no. 6, pp. 4846–4860, 2022.
- [21] F. Dörfler and F. Bullo, "Synchronization in complex networks of phase oscillators: A survey," *Automatica*, vol. 50, no. 6, pp. 1539–1564, 2014.
- [22] F. Paganini and E. Mallada, "Global analysis of synchronization performance for power systems: Bridging the theory-practice gap," *IEEE Trans. Automat. Contr.*, vol. 65, no. 7, pp. 3007–3022, 2019.
- [23] C. Yang, L. Huang, H. Xin, and P. Ju, "Placing grid-forming converters to enhance small signal stability of pll-integrated power systems," *IEEE Trans. Power Systems*, vol. 36, no. 4, pp. 3563–3573, 2021.
- [24] F. Milano and A. Ortega, "Frequency divider," *IEEE Trans. Power Syst.*, vol. 32, no. 2, pp. 1493–1501, 2016.
- [25] Y. Chen, K.-W. Lao, D. Qi, H. Hui, S. Yang, Y. Yan, and Y. Zheng, "Distributed self-triggered control for frequency restoration and active power sharing in islanded microgrids," *IEEE Trans. Ind. Inform.*, 2023.
- [26] W. Hao, Z. Huang, J. Lu, Y. Zhou, S. Liao, X. Wang, M. Chen, and D. Gan, "Structural properties of v-q jacobian matrix and voltage stability analysis of power network with photovoltaic penetration," *Proc. CSEE*, vol. 43, no. 05, pp. 1719–1730, 2023.
- [27] G. W. Stewart and J.-g. Sun, *Matrix perturbation theory*, 1990.
- [28] A. Sen, P. Ghosh, V. Vittal, and B. Yang, "A new min-cut problem with application to electric power network partitioning," *European Transactions on Electrical Power*, vol. 19, no. 6, pp. 778–797, 2009.
- [29] L. Sun, C. Zhang, Z. Lin, F. Wen, Y. Xue, M. A. Salam, and S. P. Ang, "Network partitioning strategy for parallel power system restoration," *IET Gener. Transm. Distrib.*, vol. 10, no. 8, pp. 1883–1892, 2016.
- [30] F. Dörfler, J. W. Simpson-Porco, and F. Bullo, "Electrical networks and algebraic graph theory: Models, properties, and applications," *Proc. IEEE*, vol. 106, no. 5, pp. 977–1005, 2018.
- [31] F. Bullo, *Lectures on network systems*. Kindle Direct Publishing Seattle, DC, USA, 2020, vol. 1, no. 3.
- [32] C. Canizares, T. Fernandes, E. Gerdali Jr, L. Gérin-Lajoie, M. Gibbard, I. Hiskens, J. Kersulis, R. Kuiava, L. Lima, F. Marco *et al.*, "Benchmark systems for small signal stability analysis and control," no. PES-TR, 2015.
- [33] P. S. Kundur and O. P. Malik, *Power system stability and control*. McGraw-Hill Education, 2022.
- [34] B. K. Poolla, D. Groß, and F. Dörfler, "Placement and implementation of grid-forming and grid-following virtual inertia and fast frequency response," *IEEE Trans. Power Syst.*, vol. 34, no. 4, pp. 3035–3046, 2019.